# Quantifying size distributions of nanolipoprotein particles with single-particle analysis and molecular dynamic simulations

**Craig D. Blanchette, Richard Law, W. Henry Benner, Joseph B. Pesavento, Jenny A. Cappuccio, Vicki Walsworth, Edward A. Kuhn, Michele Corzett, Brett A. Chromy, Brent W. Segelke, Matthew A. Coleman, Graham Bench, Paul D. Hoeprich, and Todd A. Sulchek[1]**

Chemistry, Materials, and Life Sciences, Lawrence Livermore National Laboratory, Livermore, CA 94551

**Abstract Self-assembly of purified apolipoproteins and phospholipids results in the formation of nanometer-sized lipoprotein complexes, referred to as nanolipoprotein particles (NLPs). These bilayer constructs are fully soluble in aqueous environments and hold great promise as a model system to aid in solubilizing membrane proteins. Size variability in the self-assembly process has been recognized for some time, yet limited studies have been conducted to examine this phenomenon. Understanding the source of this heterogeneity may lead to methods to mitigate heterogeneity or to control NLP size, which may be important for tailoring NLPs for specific membrane proteins. Here, we have used atomic force microscopy, ion mobility spectrometry, and transmission electron microscopy to quantify NLP size distributions on the single-particle scale, specifically focusing on assemblies with 1,2-dimyristoyl-*sn*-glycero-3-phosphocholine (DMPC) and a recombinant apolipoprotein E variant containing the N-terminal 22 kDa fragment (E422k). Four discrete sizes of E422k/DMPC NLPs were identified by all three techniques, with diameters centered at ~14.5, 19, 23.5, and 28 nm. Computer simulations suggest that these sizes are related to the structure and number of E422k lipoproteins surrounding the NLPs and particles with an odd number of lipoproteins are consistent with the double-belt model, in which at least one lipoprotein adopts a hairpin structure.**—Blanchette, C. D., R. Law, W. H. Benner, J. B. Pesavento, J. A. Cappuccio, V. Walsworth, E. A. Kuhn, M. Corzett, B. A. Chromy, B. W. Segelke, M. A. Coleman, G. Bench, P. D. Hoeprich, and T. A. Sulchek. **Quantifying size distributions of nanolipoprotein particles with single-particle analysis and molecular dynamic simulations.** ***J. Lipid Res.*** **2008.** 49: **1420–1430.**

**Supplementary key words** apolipoproteins • nanodiscs • high density lipoproteins • atomic force microscopy • ion mobility spectrometry

Membrane proteins are involved in numerous vital biological processes, including signal transduction, transport, adhesion, and cell-cell communication, and more recently they have become the primary targets for therapeutic drug delivery. Despite the emerging importance of membrane proteins, very few robust and versatile methods exist for the solubilization of these biological molecules. Recently, self assembling nano-scale lipoprotein particles have been identified as a potential model membrane mimetic for this purpose (1, 2). Purified apolipoproteins and lipid have been shown to self-assemble in vitro to form discoidal bilayer patches with the lipoproteins localized to the perimeter. This was first demonstrated by Jonas, Drengler, and Patterson (3) using purified apolipoprotein A-I (apoA-I). Since then, the self-assembly of these discoidal nanolipoprotein particles (NLPs) has been demonstrated for a wide range of other apolipoproteins, including apoE, apoC, apoB, and apolipohorin III (4–14). Recently, Sligar and others (1, 2, 15–17) have shown that when membrane proteins are present during NLP self-assembly, these complexes become associated with the particle, aiding in membrane protein solubilization. This new technology has been demonstrated for a subset of model membrane proteins, but a better understanding of particle size, homogeneity, and stability is essential in order to accommodate a wider range of membrane protein sizes and morphologies.

Particle heterogeneity has been widely identified for these self-assembled particles (5, 18–20), yet this phenomena has only been studied in detail by Jonas et al in the 1980s. In these studies, the existence of multiple-sized particles composed of apoA-I/1-palmitoyl-2-oleoyl-sn-glycero-3-phosphocholine (POPC)/cholesterol NLPs (21) and apoA-I/1,2-dipalmitoyl-*sn*-glycero-3-phosphocholine (DPPC)/cholesterol NLPs (6) were identified by nondenaturing gradient gel electrophoresis (GGE) (6, 21). Despite

*This work was performed under the auspices of the U. S. Department of Energy by Lawrence Livermore National Laboratory under Contract DE-AC52-07NA27344 with support from Lawrence Livermore National Laboratory (Grant 06-SI-003 awarded to P.D.H.).*

*Manuscript received 18 December 2007 and in revised form 13 March 2008.*

*Published, JLR Papers in Press, April 9, 2008.*
*DOI 10.1194/jlr.M700586-JLR200*

[1] To whom correspondence should be addressed.
e-mail: sulchek1@llnl.gov

the novel observations in this earlier work, no studies have been done subsequently to examine size heterogeneity for NLPs assembled from engineered lipoprotein constructs for use in biotechnology applications. Furthermore, this concept has not previously been systematically examined using higher resolution particle-sizing techniques.

Traditionally, size-exclusion chromatography (SEC) (15, 16), nondenaturing GGE (6, 21), small-angle X-ray scattering (SAXS) (22, 23), and transmission electron microscopy (TEM) (8, 9, 13) have been used to characterize particle size. Because SEC, GGE, and SAXS all determine particle size derived from averages of ensembles of particles, none can provide biophysical data capturing subtle differences in particle size from multiple heterogeneous populations. Single-particle sizing techniques, such as TEM, atomic force microscopy (AFM), and ion mobility spectroscopy (IMS), enable quantification of the size of individual NLPs (14), allowing the population size distribution to be examined. Such information has the potential to provide insights into the relationship between NLP size and structural composition and may prove valuable for biotechnology applications of NLPs as model membrane systems for membrane protein solubilization. For example, understanding the size distribution of different NLP assemblies may be essential for accommodating differently sized membrane proteins.

We have used AFM, TEM, and IMS as primary characterization techniques to quantify NLP heterogeneity, specifically focusing on one type of NLP assembled with 1,2-dimyristoyl-*sn*-glycero-3-phosphocholine (DMPC) and a recombinant apoE variant containing the N-terminal 22 kDa fragment (E422k). E422k was chosen for this study based on its potential importance for biotechnology applications, specifically the solubilization of membrane proteins. It is easy to purify to homogeneity and is known to be more stable than full-length apoE4 or apoE3. NLP formation with E422k is highly reproducible, and NLPs are stable over extended time periods. Furthermore, it produces larger particles compared with apoA-I or MSP1, a truncated version of apoA-I (apoA-I Δ1–22) (14), which may be relevant when accommodating larger membrane proteins. AFM was used to image individual E422k/DMPC NLPs under physiologically relevant buffer conditions, while IMS, a very sensitive and precise technique for measuring particle size (24), was used to determine size distributions for the entire NLP population. TEM was used as a third technique to further verify the size distribution obtained from AFM and IMS. All three techniques independently identified the existence of four distinct particle sizes of E422k/DMPC NLPs with diameters centered at ~14.5, 19, 23.5, and 28 nm. Initial computer modeling and molecular dynamics (MD) simulations indicate that these sizes may be related to a quantized number of the E422k lipoproteins surrounding the NLPs. Discrete sizes were also observed in NLPs formed from apoA-I/DMPC, E422k/1,2-dioleoyl-*sn*-glycero-3-phosphocholine (DOPC), and NLPs purchased from Nanodisc, Inc., indicating that distribution of discrete NLP sizes is likely a general phenomenon.

## MATERIALS AND METHODS

### Materials

DMPC and DOPC were purchased from Avanti Polar Lipids, Inc. (Alabaster, AL). Full-length apoA-I was purchased from Fitzgerald, Inc. (Concord, MA), Nanodisc™ particles were purchased from Nanodisc, Inc. (Urbana, IL).

### E422k protein production

The expression clone to produce E422k, the N-terminal 22 kDa fragment of apoE4, as a 6His and thyrodoxin-tagged construct was kindly provided by Dr. Karl Weisgraber. The production and purification of E422k have been described in detail elsewhere (14).

### NLP formation

NLP formation and purification have been described in detail elsewhere (14). Briefly, dried DMPC was dissolved in 10 mM Tris, pH 7.4, 0.15 M sodium chloride, 0.25 mM EDTA, 0.005% sodium azide (TBS) buffer at a concentration of 20 mg/ml followed by probe sonication to clarity. This resulting liposome suspension was spun at 13,000*g* for 2.5 min to remove any residual titanium from the probe sonicator and unsolubilized lipid. E422k (200–250 μg) was added to the TBS/DMPC solution at a mass ratio of 4:1. The particle formation process was started with three repeated sets of transition temperature incubations, above (10 min at 30°C) and below the transition temperature of DMPC (23.8°C), followed by incubation at 23.8°C overnight. The NLPs were purified by SEC using a Superdex 200 HR 10/300 column (GE Healthcare), in TBS at a flow rate of 0.5 ml/min. The NLP fractions were concentrated to ~0.1 mg/ml using molecular mass sieve filters (Vivascience) with molecular mass cutoffs of 50 kDa. Protein concentration was determined using the ADV01 protein concentration kit (Cytoskeleton, Inc.).

### AFM

Atomically flat Muscovite mica discs were glued to metal substrates to secure them to the scanner of a stand-alone MFP-3D atomic force microscope (Asylum Research, Santa Barbara, CA). Two microliters of solution at 1.0 μg/ml concentration was incubated for 2 min on the mica surface in imaging buffer (10 mM $MgCl_2$, 10 mM Tris-HCl, and 0.1 M NaCl, adjusted to pH 8.0), then lightly rinsed. The atomic force microscope has a closed stage loop in the x, y, and z axes. Topographical images were obtained with silicon nitride cantilever probes (Microlever sharpened contact tip; Veeco, Santa Barbara, CA) with a spring constant of 0.05 N/m. Images were taken in alternate contact mode in liquid, with amplitudes of <20 nm and an amplitude set point at 50% tapping amplitude. Scan rates were <1.5 Hz. Height, amplitude, and phase images were recorded. Diameters of particles in images were determined by the full-width half-maximum analysis of contiguous particles in the slow scan direction, using IgorPro Wavemetrics software routines. Heights of particles were determined from histogram analysis. Experiments were carried out in a temperature-controlled room at 23 ± 1°C.

Alternate contact mode or tapping mode was used in AFM imaging to ensure minimal structural perturbation from tip sample contact force. It is widely known that imaging nano-scale particles by AFM results in laterally broadening particle size due to tip convolution effects, but there exists a second broadening effect due to the finite response of imaging feedback in the fast scan direction (25). This latter effect can result in NLP shape appearing elongated in the fast scan direction. To limit tip convolution effects, only tips revealing sharp imaging were used for analysis. To limit the broadening from slow imaging response, full-width half-maximum from a cross-section perpendicular to

the fast scan direction was used to determine particle diameter. To determine the reproducibility of the procedure for measuring NLP diameters, randomly selected particles were repeatedly imaged to verify consistent diameter measurements.

### IMS

IMS determines the mean aerodynamic diameter of particles based on the terms in equation 1:

$$D_p = nqE/3\pi\eta v \qquad (Eq.\ 1)$$

where $D_p$ = particle aerodynamic diameter, n = number of elementary electrical charges, q = unit charge in coulombs, E = electrical field strength, $\eta$ = viscosity of suspending gas, and v = particle velocity. This is a first principles measurement and it does not require calibration for measuring particle diameter. The development of an electrospray interface provides a way to analyze particles suspended in a liquid. We used an electrospray interface (model 3480; TSI, Inc., Shoreview, MN) and a Macroion Mobility Spectrometer (model 3890; TSI, Inc.) to measure the size distribution of NLP particles after they were exchanged via dialysis into a 25 mM ammonium acetate buffer (14, 26, 27). The methodology used to prepare the samples and measure the NLP size distributions were similar to a method developed by Benner and colleagues (14, 26, 27) for analyzing human lipoprotein particles and NLPs.

NLP aerodynamic diameters were subsequently converted to aerodynamic spherical volumes. Assuming volume equivalency of the aerodynamic spherical volumes and NLP discoidal volumes and using an appropriate correction factor, IMS-derived mean aerodynamic diameters were converted to NLP discoidal diameters through

$$d_{NLP} = 2\sqrt{\frac{4(K\,R_{ma})^3}{3\,h}} \qquad (Eq.\ 2)$$

where $d_{NLP}$ is the NLP discoidal diameter, h is the NLP discoidal height determined through AFM analysis, $R_{ma}$ is the mean spherical radius determined from IMS, and K is an appropriate correction factor. It is appropriate to convert aerodynamic spherical diameter to discoidal diameters with this factor because the net velocity of the particles during analysis is slow ($\sim$5 cm/s) compared with their diffusional velocity (440 cm/s), and thus their shape will be slightly distorted during differential mobility analysis.

### TEM

NLP samples were diluted using TBS, mounted onto carbon-coated 400 mesh copper electron microscopy grids, stained with 2% uranyl acetate, and imaged using a Philips CM300 FEG transmission electron microscope operating at an accelerating voltage of 300 keV, as described previously (14).

### Native PAGE

Equal amounts of NLP samples (0.5–2 μg) were diluted with 2× native gel sample buffer (Invitrogen) and loaded onto 4–20% gradient premade Tris-glycine gels (Invitrogen). Samples were electrophoresed for 250 V h (Bio-Rad) at a constant 125 V. After electrophoresis, gels were incubated with Sypro Ruby for 2 h and then destained using 10% methanol and 7% aqueous acetic acid. Following a brief wash with double distilled water, gels were imaged using a Typhoon 9410 (GE Healthcare) at 532 nm (green laser) with a 610 nm bandpass 30 filter. Molecular weights were determined by comparing migration versus log molecular weight of standard proteins found in the NativeMark standard (Invitrogen).

### NLP modeling and molecular dynamics

An idealized 35 × 35 $nm^2$ bilayer slab of DMPC lipids (a 740,000 atom system) was created and equilibrated to give a lipid cross-sectional area of 52 $Å^2$ per lipid (15). Circular discs were cut out of this slab at 0.5 nm diameter increments, in a range of 11 to 30 nm. The E422k crystal structure, PDB:1GS9 (28), was used as the basis for the protein modeling.

Refolded E422k proteins were modeled and tested in three different forms: fully extended, doubled back/"hairpin," and

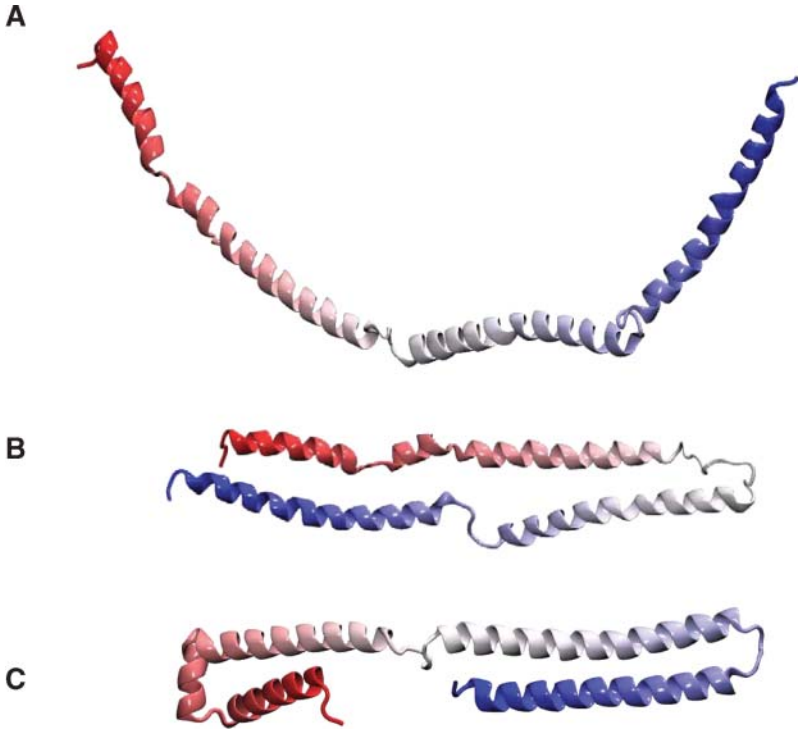


**Fig. 1.** Refolded apolipoprotein E variant containing the N-terminal 22 kDa fragment (E422K) proteins were generated in three different forms: fully extended (A), doubled back/hairpin (B), and semi-extended/double-hairpin (C) folds.

semiextended/"double-hairpin" folds (**Fig. 1**). Initial modeling of the NLPs was based on a fully extended E422k (Fig. 1A), assuming that E422k NLPs would be similar to the "double-belt" model reported for apoA-I NLPs (29–32) and suggested previously for E322K NLPs (33). This gave rise to a fold for E422k, with full hydrophobic association for the lipid, that is fully extended, as suggested previously for this portion of apoE4 (10). However, at least two other folds are possible for E422k, consistent with water exclusion of the hydrophobic acyl chains. The soluble folded E422k contains three hairpin turns linking four helices (34). Forming a hairpin in the extended fold so that the apoE4 doubles back on itself creates a model with a self-contained double belt (Fig. 1B). This so-called hairpin model for lipoproteins has been suggested previously (35). For this fold to form, the loop between helices 2 and 3 of folded E422k would have to undergo a 180° rotation. A more energetically favorable rearrangement of E422k would involve only the opening of the helix 2–3 loop to produce a semiextended double-hairpin model, that is, one containing two of the bends from the folded E422k and involving a simple opening of the hydrophobic core of the folded E422k to pack against the hydrophobic face of the lipid (Fig. 1C).

Proteins were aligned along the equator of the lipid disc and packed against the lipid discs of different sizes with the aim of fully enclosing the hydrophobic face of the lipids but not allowing the proteins to overlap each other. A 1 ns equilibration MD run was then used to optimize the packing of the lipid against the protein. NLPs without gaps between lipid and protein were then entered into a 40 ns MD simulation to determine the stability of the model. All MD simulations were run using the CHARMM force field (36) in NAMD (37), with many of the settings and setup details taken from previous simulations (38, 39). Simulations were conducted on 1,024 processors of Thunder, a 23 teraflop, 4096 Intel Itanium2 processor machine at the Livermore Computing Center. System setup, analysis, and image preparation was done using Gromacs (40), Pymol, and VMD (41), with additional "in-house" tcl/tk, perl, and C++ scripts.

## RESULTS

### NLP formation, purification, and individual particle characterization

E422k/DMPC NLPs were formed using DMPC as the lipid component and E422k as the lipoprotein component. A typical SEC trace of an E422k/DMPC NLP assembly contains three dominant peaks, the free lipid-rich peak, an NLP-rich peak, and an apolipoprotein-rich peak (**Fig. 2**) (9, 14). NLP-rich fractions collected from SEC were pooled and then used for further characterization by AFM and TEM (Fig. 2B, C). Both single-particle characterization techniques showed the production of 12–30 nm NLPs (Fig. 2B, C). The AFM image in Fig. 2B illustrates the broadening effect in the fast scan direction, described in Materials and Methods, which can be observed due to the finite response of imaging feedback in this direction. From the TEM images and AFM cross-sectional analysis

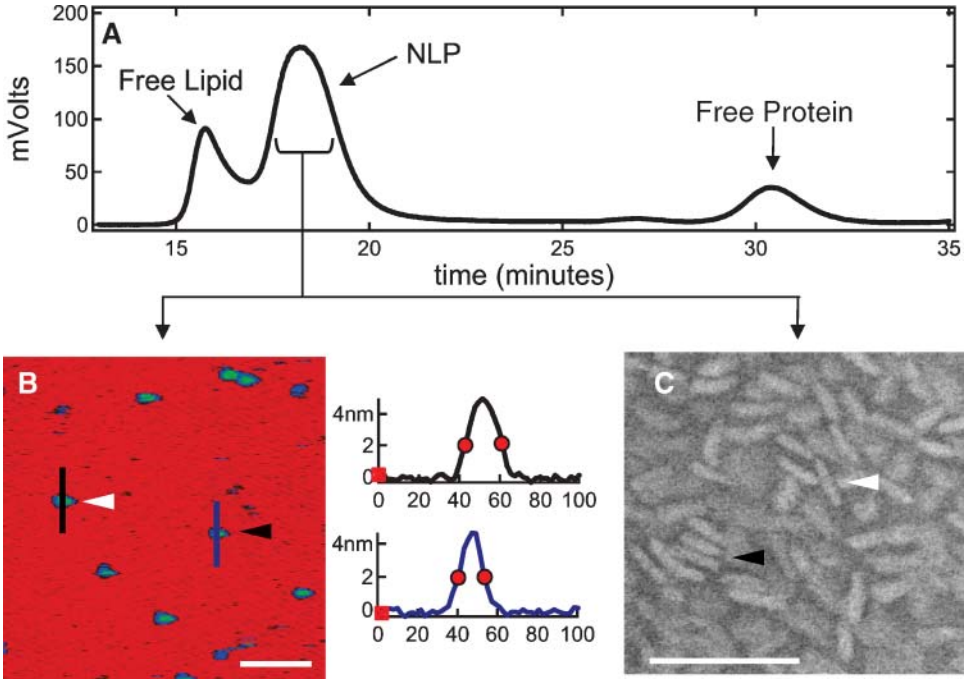


**Fig. 2.** Method of purification and characterization of self-assembled nanolipoprotein particle (NLPs). A: Size-exclusion chromatography (SEC) trace of E422K/1,2-dimyristoyl-*sn*-glycero-3-phosphocholine (DMPC) NLPs. B, C: Atomic force microscopy (AFM; B) and transmission electron microscopy (TEM; C) images of E422K/DMPC NLPs after formation and purification. Cross-sectional analysis of AFM images (the black and blue lines in the image correspond to the black and blue cross-sectional traces shown to the left) was used to measure NLP height and diameter. The red circles in the traces correspond to the full-width half-maximum points used to determine particle diameter. Arrowheads in the AFM and TEM images point to NLPs of differing diameters, indicating size heterogeneity (black arrowheads point to smaller NLPs and white arrowheads point to larger NLPs). AFM bar = 100 nm; TEM bar = 50 nm.

shown in Fig. 2B, C, it is quite apparent that E422k/DMPC NLPs exhibit particle size heterogeneity.

### Heterogeneous E422k/DMPC NLP diameter distributions display discrete sizes, as determined by AFM, TEM, and IMS

AFM cross-sectional analysis of several hundred single NLPs was used to quantify both height and diameter heterogeneity. The height distribution of the particles revealed a relatively homogeneous population displaying a Gaussian distribution, with a mean height of 4.9 ± 0.2 nm, consistent with the height of a lipid bilayer. However, histograms of the diameters revealed that the NLP sizes displayed discrete diameters (**Fig. 3**). The discrete diameters were centered at 14.7, 18.8, 23.3, and 28.7 nm, and the fraction of each NLP type decreased with increasing NLP diameters (**Table 1**).

To verify that the observed discrete diameters were not an effect of AFM tip resolution or mica surface-particle interactions, E422k/DMPC NLPs were also analyzed by IMS and TEM (**Fig. 4**). IMS is a technique that determines the mean aerodynamic diameter of particles based upon the differential migration of gas phase ions through a homogeneous electric field and is well established in the field of aerosol science for particle analysis and measurement. The history of the development of IMS was recently extensively reviewed (42). In fact, IMS has been used to determine size distributions for HDLs, LDLs, and VLDLs (26, 27) and more recently for NLPs assembled from a wide range of lipoproteins (14). The IMS traces confirm the discrete NLP diameters seen with AFM; in fact, the diameter peaks by both AFM (14.9, 18.7, 23.3, and 28.7 nm) and IMS (14.1, 19.5, 24.3, and 28.6 nm) are almost identical. TEM also confirmed the existence of the same four discrete sizes that were observed by AFM and IMS (14.9, 18.9, 23.3, and 29.0 nm) (Fig. 4C). The heterogeneous discrete diameters observed by IMS, AFM, and TEM indicate that these sizes are not due to an AFM tip convolution affect but rather represent the real diameter distribution. Interestingly, each peak is separated by rather larger set sizes of ~4–5 nm in diameter, which suggests at least three possibilities: a change in tertiary structure of the surrounding lipoprotein E422k, variation in the number of E422k lipoproteins per particle, or a combination of these two effects.

### Native gel electrophoresis and the effects of cholate on E422k/DMPC NLP separation

E422k/DMPC NLPs were subjected to native gel electrophoresis to further assess particle heterogeneity. Cholate at 0 and 5 mM (below the critical micelle concentration of ~15 mM) was added to the NLP solution after assembly and run on a native gel (**Fig. 5A**). The addition of no cholate resulted in a single band at ~603 kDa, despite observing multiple sizes by AFM, IMS, and TEM (Fig. 5A). In the presence of 5 mM cholate, native gel analysis revealed four bands at 234, 312, 458, and 615 kDa. To determine whether the addition of cholate resulted in the disassembly of NLPs or altered NLP size distribution, the sample was imaged by AFM both before (Fig. 5B) and after (Fig. 5C) cholate addition, and no significant changes were observed in either NLP height or diameter distribution.

### MD simulations of E422k/DMPC NLPs

To determine whether the discrete NLP diameters observed by AFM, TEM, and IMS could be related to the number of E422k proteins in an NLP, NLP assembly was computationally modeled using MD simulations. Modeling of NLPs using fully extended double-belted E422k proteins (Fig. 1A) could produce NLPs of diameter 14.5 and 23.5 nm, respectively, containing four and six copies of the E422k protein (**Fig. 6**). The extended conformation of the E4 protein implies that the protein must be added in pairs to produce a double belt and fully satisfy the hydrophobic matching required to stabilize the disc of lipid.

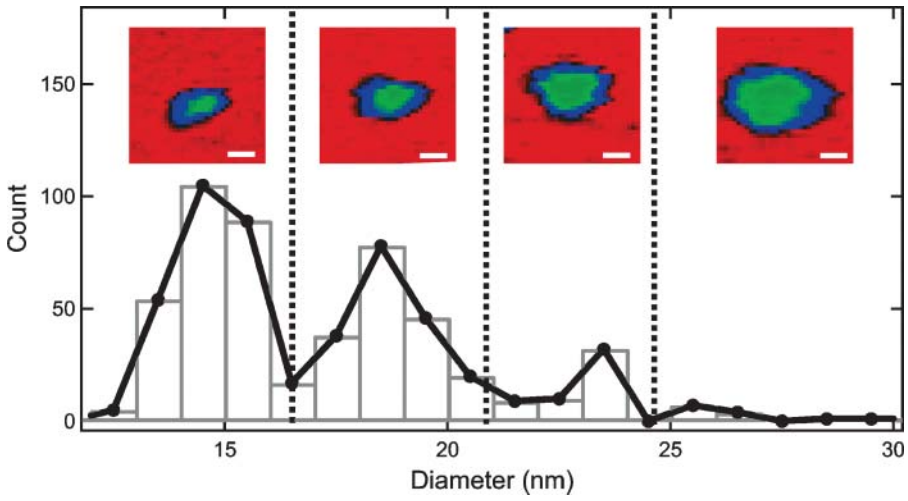


**Fig. 3.** NLP diameter distribution for 1,000 NLPs with a bin width of 1.0 nm. NLPs contain at least four distinct populations with diameter sizes of 14.7, 18.8, 23.3, and 28.7 nm (see Table 1 for mean, SD, and percentage of each size). The insets show AFM images of the four differently sized NLPs. Bars = 10 nm.

TABLE 1. Diameter mean, SD, and percentage of the four NLP populations

| Variable | NLP Type 1 | NLP Type 2 | NLP Type 3 | NLP Type 4 |
|---|---|---|---|---|
| Diameter (nm) | 14.7 ± 0.9 | 18.8 ± 1.0 | 23.3 ± 1.1 | 28.7 ± 1.5 |
| Fraction | 0.56 | 0.33 | 0.10 | 0.02 |

NLP, nanolipoprotein particle.

Therefore, modeling could not reproduce NLPs with diameters of 19 and 28 nm using fully extended double-belted E422k proteins.

Interestingly, MD simulations revealed that stable NLPs with diameters of 14.5, 19, 23.5, and 28 nm could all be formed using the hairpin (Fig. 1B) and double-hairpin (Fig. 1C) models of E422k (Fig. 6). Furthermore, simulations revealed that the 19 and 28 nm NLPs, respectively, contain five and seven E422k proteins, with at least one of the proteins, if not more, forming a hairpin or double hairpin. In addition, MD simulations revealed that NLPs formed from hairpin, double-hairpin, and extended models of E422k have similar stability, with full hydrophobic matching at satisfactory lipid-protein ratios as the most important factor for stability. This suggests the possibility that any one NLP can contain E422k proteins in any one or more of the three different folded forms (Fig. 1). The only constraint is that the 19 and 28 nm NLP are unlikely to be formed from the E422k scaffold that is only in the extended conformation. Figure 6 summarizes the modeling of particle sizes and reveals that the simulations were able to verify the experimental size data yielding the following size-protein number-lipid number ratios: 14.5 nm:4:433, 19 nm:5:783, 23.5 nm:6:1,270, and 28 nm:7:1,780. A more detailed presentation of the results of the MD simulations is currently the focus of a manuscript in preparation.

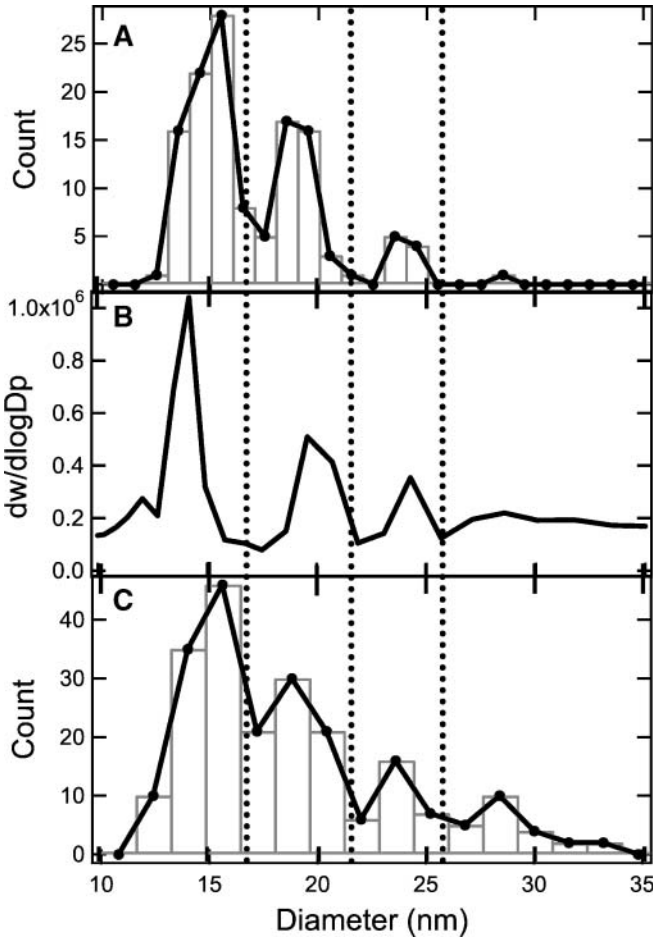


**Fig. 4.** Comparison of diameter distributions measured by AFM, IMS, and TEM. A: NLP diameters determined through AFM binned at 1 nm. B: NLP diameters determined through IMS. C: NLP diameters determined through TEM binned at 1.6 nm.

**Discrete NLP diameters were also observed in apoA-I/DMPC NLPs, E422k/DOPC, and NLPs purchased from Nanodisc, Inc.**

To determine whether the formation of discrete NLP diameters was a general phenomenon for self-assembling NLPs, size distributions were analyzed by AFM for apoA-I/DMPC NLPs, and NLPs (16) purchased from Nanodisc, Inc. ApoA-I/DMPC NLPs were formed with the same procedure used for E422k/DMPC NLPs, with the exception that cholate was added during assembly (14). The purchased NLPs were formed from MSP1 and DMPC. The diameter histogram for the two different samples clearly show discrete peaks similar to those observed in E422k/DMPC NLPs, except with a shift to slightly smaller particle diameters (**Fig. 7A, B**). The diameter peaks for the purchased NLPs and apoA-I/DMPC NLPs were 12.8, 17.2, 21.9, and 26.6 nm and 13.4, 17.4, 21.6, and 25.5 nm, respectively. The shift to smaller diameters is expected, since both apoA-I and its recombinant derivatives have been shown to form smaller particles (14). To ascertain the effect of the lipid on the discrete size distributions observed for E422k, NLPs were assembled with DOPC instead of DMPC (Fig. 7C). Under these conditions, not only were the discrete NLP diameter sizes the same as those observed for E422k/DMPC NLPs, but the relative amount of each size was similar. Our results indicate that the formation of discrete sizes for lipoprotein/lipid self-assembly into NLPs may be a general phenomenon.

## DISCUSSION

Using AFM imaging of single NLPs, we have shown that the self-assembly of E422k/DMPC NLPs results in particle size distributions that display discrete diameters centered at 14.7, 18.8, 23.3, and 28.7 nm (Table 1). In addition, TEM and IMS verified these AFM results, eliminating the possibility that these quantized peaks observed by AFM are due to either a tip convolution effect or tip-sample interactions (Fig. 4). Although the AFM, TEM, and IMS techniques complement one another, they offer a distinct advantage when they are applied to study one system, because it allows for both single-particle imaging and analysis of a subpopulation (AFM and TEM) and whole sample analysis (IMS); thus, one can understand the system at the single-particle level while not losing whole sample statistical data. It is worth noting that the close match in absolute NLP diameter

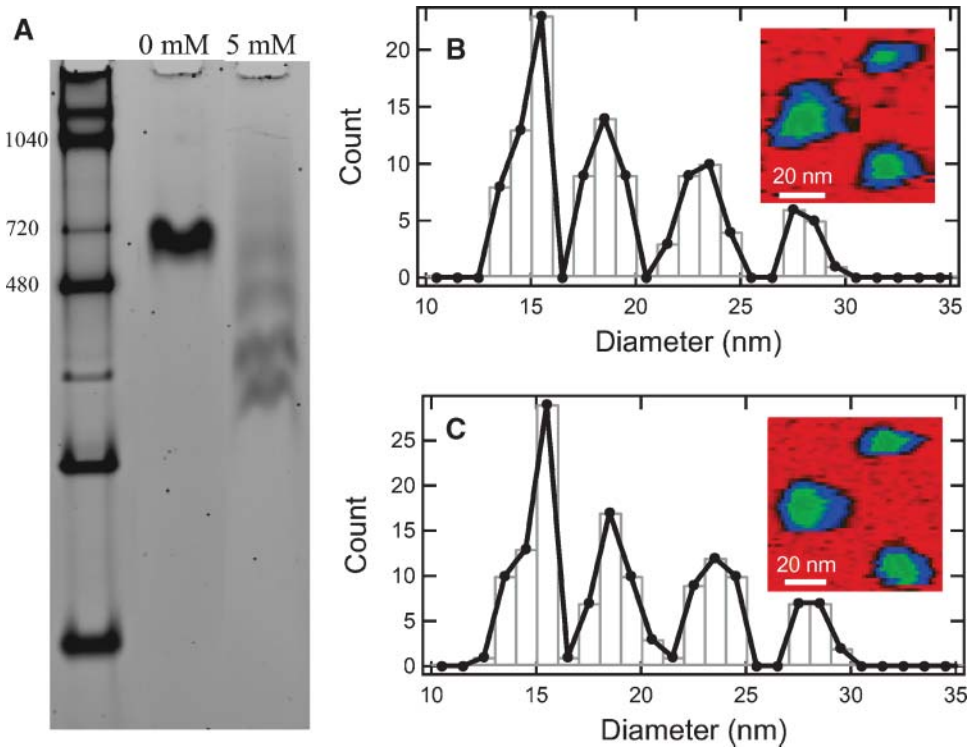


**Fig. 5.** Effect of cholate on NLP separation by native gel electrophoresis. A: Native gel electrophoresis of NLPs after SEC purification in the presence of 0 mM cholate (lane 2) displayed a single band, but in the presence of 5 mM cholate (lane 3) four dominant bands were observed. B: Diameter distributions of NLPs in A at 0 mM cholate. C: Diameter distributions of NLPs in A at 5 mM cholate. All histograms were binned at 1.0 nm, and AFM images were stitched together to show the predominant NLP sizes.

between IMS, TEM, and AFM indicates little to no AFM tip convolution effect that would cause artificial diameter broadening. Based on the structure of the E422k modeled through the MD simulations, we hypothesize that this lack of broadening may be due to tip geometry. Assuming a tip diameter of ~8–10 nm, we have calculated that the bulk of the lipoprotein does not contact the AFM tip during scanning, due to a gap formed from the finite radius of curvature of the AFM tip. Therefore, the NLP diameters imaged by AFM only capture the bilayer region of the NLP. Using the bilayer diameters (i.e., NLP area minus the E422k area) determined in the MD simulation, we calculated a tip convolution effect of ~2–3 nm, which is the expected value for an AFM tip diameter of ~8–10 nm.

The relative percentage of each E422k/DMPC NLP size was highly reproducible when assembled at a 1:4 E422k-to-lipid mass ratio; thus, this distribution may reflect an equilibrium distribution. It has been shown that the diameter of apoA-I NLPs increases with an increase of the lipid-to-apoA-I ratio (43). This observation is consistent with the hypothesis that changing the protein-to-lipid ratio may shift the size distribution of NLPs.

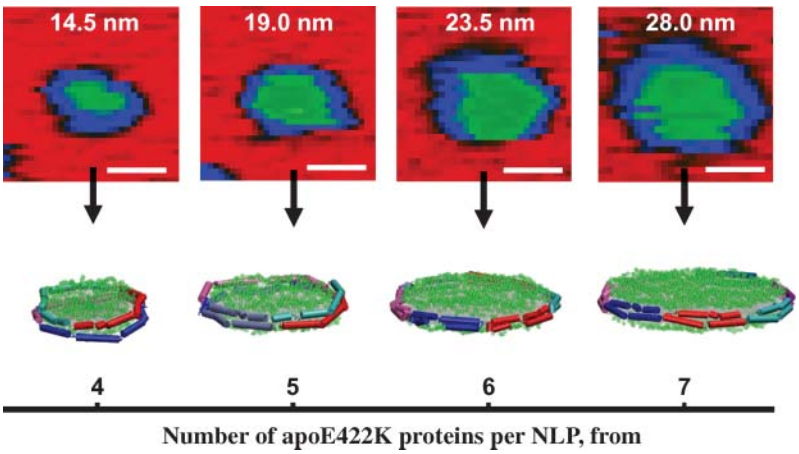


**Fig. 6.** Modeling and molecular dynamics simulations of E422k/DMPC NLP sizes observed through AFM, IMS, and TEM. Computer modeling of E422k/DMPC NLPs revealed that the multiple sizes were stable, where all the hydrophobic faces of the lipid disc were matched by the protein numbers, sizes, and stoichiometry. A double-belt model was assumed, but this criterion was satisfied by three protein folds: extended, hairpin, and double-hairpin folds. NLPs containing an odd number of E422k, the 19 nm NLPs (five scaffold), and the 28 nm NLPs (seven scaffold) were only stable if at least one E422k adopted either the hairpin or double-hairpin motif. E422K motifs in the simulated image are as follows: 14.5 nm, all extended; 19 nm, two extended, one hairpin; 23.5 nm, all double hairpin; and 28 nm, all hairpin. AFM bars = 10 nm.

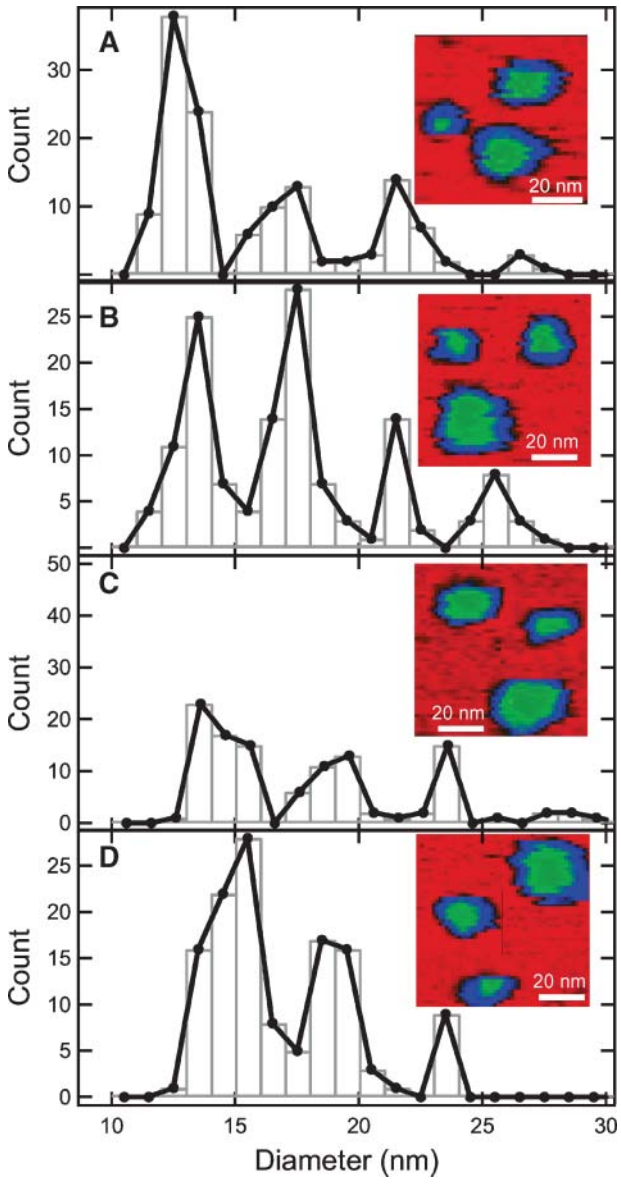


**Fig. 7.** Comparison of diameter distributions showing size heterogeneity of NLPs formed with different apolipoproteins. A: Diameter distributions of NLPs purchased from Nanodisc, Inc. (constituents MSP1/DMPC). NLPs displayed quantified diameters of 12.8 ± 0.7, 17.2 ± 1.1, 21.9 ± 0.7, and 26.6 ± 0.1 nm. B: Diameter distributions of apolipoprotein A-I/DMPC NLPs. NLPs displayed quantified diameters of 13.4 ± 0.8, 17.4 ± 0.8, 21.6 ± 0.4, and 25.5 ± 0.7 nm. C: Diameter distributions of E422k/DOPC NLPs. NLPs displayed quantified diameters of 14.6 ± 0.9, 19.0 ± 0.8, 23.5 ± 0.7, and 28.3 ± 0.7 nm. D: Diameter distributions of E422k/DMPC NLPs. All histograms were binned at 1.0 nm, and AFM images were stitched together to show the predominant NLP sizes.

The structure of fully intact apoE contains two independently folded domains: a 22 kDa N-terminal domain, which is responsible for LDL receptor binding, and a 10 kDa C-terminal domain, which contains lipid binding elements required for the formation of spherical lipoprotein particles (44–46). The crystal structure for the lipid-free state of the 22 kDa domain (truncated apoE4 used in this study) reveals a structure consisting of a four-helix bundle in which each helix is amphipathic with its hydrophobic face orientated toward the center of the bundle (34, 47). It has been shown that assembly of discoidal NLPs from E422k involves a series of steps including initial interaction, lipid-triggered opening of the four-helix bundle, and further reorganization of the helices to achieve the final lipid-bound discoidal conformation (9). Although the structural organization of E422k around the discoidal particle was not determined in this study, it was suggested that the assembly process may involve opening up of the four-helix bundle (9). Recently, Raussens et al. (33) used Fourier transform infrared spectroscopy-ATR and linear dichroism to study the structure of E322k/DMPC reconstituted-HDLs. From this analysis, they provided the first experimental evidence that the E322k helices are orientated perpendicular to the acyl chains of the lipid in discoidal complexes, consistent with the belt model. This was further supported by a more recent study in which Narayanaswami et al. (48) examined the ability of spatially defined nitroxide-labeled phosopholipids to quench the fluorescence of unique single tryptophan apoE3 variants in r-HDL. In addition, a large body of evidence indicates that apoA-I in discoidal HDLs adopt conformations consistent with the belt model (49–52). Since the sequence of apoE is 44% similar to that of apoA-I and has a similar pattern of 11 and 22 amino acid tandem repeat sequences, it is likely that E422k adopts a similar conformation in NLPs.

To elucidate the relationship between the experimentally observed discrete sizes and NLP structure, NLP assemblies were computationally modeled using MD simulations assuming the belt model discussed above. From these simulations, it was determined that the ~4.5 nm diameter separation between each discrete particle is consistent with one additional E422k lipoprotein for each discrete step in increased diameter and an equivalent increase in lipid content within the particle. If an extended conformation were the only conformation available to the protein, with the proteins stacked on top of each other to give the double belt, as shown previously for apoA-I (32), the 19 and 28 nm NLP sizes would not be available to E422k-containing NLPs, assuming that all of the protein and lipid hydrophobic faces are matched. Thus, other folded states were computationally modeled and determined to be possible for the formation of NLPs: a hairpin (Fig. 1B), and a double hairpin (Fig. 1C), which are folds that allow a double belt from a single protein and an odd number of proteins to be completely packed in an ordered NLP. Recently, the structure of E422k/DPPC NLPs was determined at 10 Å resolution (53, 54). From this work, it was shown that the E422k fold was consistent with a helical hairpin (Fig. 1B), providing experimental evidence of the existence of the hairpin structures computationally modeled in this study (54, 55). Although our initial modeling efforts have focused on the double-belt model, there is much conjecture on the nature of the lipid-protein interactions. For instance, Schneeweis et al. (56) have suggested that, in addition to the helices orientated perpendicularly around the perimeter of the particles, lipoproteins may also be associated with the face of

the particle. Although these conclusions offer additional insight into potential lipid head group-lipoprotein interactions, they do not affect the major results presented here, since the focus of this work was on the perimeter of the particle.

Modeling, MD simulations and experiments have also revealed ~10% flexibility in the diameter of NLP constructs, which is possible due to the intrinsic flexibility of the lipoprotein scaffold (57). The loops in between the helices that make up the E422k fold can be more or less extended, and the gaps between adjacent E4 proteins can fluctuate as the NLP fluctuates in size and shape. This flexibility and variability may partially explain the narrow spread of the particle sizes around the 14.5, 19, 23.5, and 28 nm mean NLP diameters observed in Figs. 3, 4. A more extensive investigation using MD simulations of E422k NLPs is currently being pursued.

Native gel electrophoresis often has been used as a primary method for NLP size characterization (3, 4, 6, 21, 57–59); however, E422k/DMPC NLPs display a single band, while multiple-sized species were consistently observed by AFM, IMS, and TEM. This discrepancy was shown to be mitigated by the addition of cholate to the NLP solution after assembly, where at 5 mM cholate four bands were observed (Fig. 5A). These results suggest that in the absence of cholate, NLPs may interact with one another during electrophoresis such that differently sized NLP particles migrate to the same spot on the native gel (~620 kDa). Alternatively, in the absence of cholate, the process of electrophoresis may result in the degradation of smaller NLPs. Owing to its negative charge, the addition of cholate may afford a mechanism for enhanced NLP stability or alternatively a mechanism that disrupts NLP interactions during native gel electrophoresis. An additional discrepancy observed was the measured molecular masses of the differently sized particles. From the MD simulations, the molecular masses for the four particles were calculated to be 293, 531, 861, and 1207 kDa, respectively, but the four bands on the native gel corresponded to molecular masses of 234, 312, 458, and 615 kDa, respectively. From this analysis, it appears that as the particles get larger, these two numbers increasingly deviate. We believe that this occurs because sizing by native gel electrophoresis is based on comparison with standards that are globular in shape and not discoidal; therefore, NLPs with larger diameters will deviate to a greater extent in shape and migration behavior from these spherical standards (i.e., for larger diameter-to-height aspect ratios). In addition, since cholate is in the loading buffer, it may also affect migration relative to the globular standards. Furthermore, the major constituent of these particles is lipid, and the migration of lipid-rich species on a gel may be much different than that of globular protein standards.

We also observed the formation of multiple discretely sized particles for apoA-I/DMPC NLPs and NLPs purchased from Nanodisc, Inc. (Fig. 7), which indicates that this may be a general result for self-assembling NLPs. The purchased NLPs from Nanodisc, Inc. imaged in this study have been previously reported to be relatively homogeneous in size (i.e., all particles exhibited one definitive size) (16, 23). However, the NLPs shown in Fig. 7A exhibit the characteristic discrete diameter size distributions seen in apoA-I and E422k NLP preparations (14). It has been shown that optimal MSP1-to-DMPC lipid ratios and multiple SEC purification steps are required for the formation of more homogeneous populations of nanodiscs (15, 16); thus, it is plausible that the purchased NLPs were not self-assembled or purified under these optimal conditions. Another plausible reason for this difference is the method of size characterization used in the above studies: SAXS determines particle size derived from an average of ensembles of particles, rather than the single-particle characterization techniques employed here; as a result, SAXS may be relatively insensitive in capturing differences in size from multiple heterogeneous populations.

Discrete and heterogeneous particle sizes was first observed by Jonas et al for apoA-I/POPC/cholesterol r-HDLs (21) and apoA-I/DPPC/cholesterol r-HDLs (6). In those work, the authors isolated differently sized particles through fractionation on a Superose 6 column and sizes were determined by nondenaturing GGE (6, 21). From those studies, three distinct stable particle sizes were identified for apoA-I/DPPC/cholesterol r-HDLs (9.7, 13.6, and 18.6 nm) (6) and four distinct particle sizes were identified for apoA-I/POPC/cholesterol HDLs (7.7, 8.6, 9.6, and 10.9 nm) (21). This earlier work was the first detailed study in which the existence of discrete particle sizes was identified and characterized for the in vitro assembly of discoidal lipoprotein particles. The work presented here extends these results using high-resolution imaging techniques such as AFM, IMS, and TEM and identifies a similar trend for an engineered apolipoprotein construct. In addition, by combining the sizing data with initial computational modeling, we were able to make a direct comparison between experimental data and computational simulations. From this combined approach, we were able to relate the observed discrete NLPs sizes to both lipoprotein conformational structure and quantified number of lipoproteins per particle. NLP complexes show promise as a robust platform for the stabilization of membrane proteins by overcoming many of the difficulties associated with studying membrane proteins in aqueous environments, including their inherent insolubility and self-aggregation. Further success of this technology may depend on a better understanding of particle size, homogeneity, and stability, which can be elucidated through the combination of techniques and results presented in this study.

The authors are grateful to Drs. Karl Weisgraber and Robert Ryan for helpful discussions and for providing reagents. The authors acknowledge the support of Prof. Holland Chang at the Advanced Microscopy Center at the University of California Davis.

## REFERENCES

1. Bayburt, T. H., and S. G. Sligar. 2003. Self-assembly of single integral membrane proteins into soluble nanoscale phospholipid bilayers. *Protein Sci.* **12:** 2476–2481.

2. Bayburt, T. H., Y. V. Grinkova, and S. G. Sligar. 2006. Assembly of single bacteriorhodopsin trimers in bilayer nanodiscs. *Arch. Biochem. Biophys.* **450:** 215–222.
3. Jonas, A., S. M. Drengler, and B. W. Patterson. 1980. 2 types of complexes formed by the interaction of apolipoprotein A-I with vesicles of l-alpha-dimyristoylphosphatidylcholine. *J. Biol. Chem.* **255:** 2183–2189.
4. Garda, H. A., E. L. Arrese, and J. L. Soulages. 2002. Structure of apolipophorin III in discoidal lipoproteins—interhelical distances in the lipid-bound state and conformational change upon binding to lipid. *J. Biol. Chem.* **277:** 19773–19782.
5. Jonas, A. 1986. Reconstitution of high density lipoproteins. *Methods Enzymol.* **128:** 553–582.
6. Wald, J. H., E. S. Krul, and A. Jonas. 1990. Structure of apolipoprotein A-I in three homogeneous, reconstituted high-density-lipoprotein particles. *J. Biol. Chem.* **265:** 20037–20043.
7. Jonas, A., S. A. Sweeny, and P. N. Herbert. 1984. Discoidal complexes of A and C apolipoproteins with lipids and their reactions with lecithin-cholesterol acyltransferase. *J. Biol. Chem.* **259:** 6369–6375.
8. Zorich, N., A. Jonas, and H. J. Pownall. 1985. Activation of lecithin-cholesterol acyltransferase by human apolipoprotein E in discoidal complexes with lipids. *J. Biol. Chem.* **260:** 8831–8837.
9. Lu, B., J. A. Morrow, and K. H. Weisgraber. 2000. Reorganization of the four-helix bundle of human apolipoprotein E in binding to phospholipid. *J. Biol. Chem.* **275:** 20775–20781.
10. Hatters, D. M., C. A. Peters-Libeu, and K. H. Weisgraber. 2006. Apolipoprotein E structure: insights into function. *Trends Biochem. Sci.* **31:** 445–454.
11. Gursky, O., Ranjana, and D. L. Gantz. 2002. Complex of human apolipoprotein C-1 with phospholipid: thermodynamic or kinetic stability? *Biochemistry.* **41:** 7373–7384.
12. Wientzek, M., C. M. Kay, K. Oikawa, and R. O. Ryan. 1994. Binding of insect apolipophorin III to dimyristoylphosphatidylcholine vesicles—evidence for a conformational change. *J. Biol. Chem.* **269:** 4605–4612.
13. Herscovitz, H., M. Hadzopoulouc1adaras, M. T. Walsh, C. Cladaras, V. I. Zannis, and D. M. Small. 1991. Expression, secretion, and lipid-binding characterization of the N-terminal 17% of apolipoprotein-B. *Proc. Natl. Acad. Sci. USA.* **88:** 7313–7317.
14. Chromy, B. A., E. Arroyo, C. D. Blanchette, G. Bench, H. Benner, J. A. Cappuccio, M. A. Coleman, P. T. Henderson, A. K. Hinz, E. A. Kuhn, et al. 2007. Different apolipoproteins impact nanolipoprotein particle formation. *J. Am. Chem. Soc.* **129:** 14348–14354.
15. Denisov, I. G., Y. V. Grinkova, A. A. Lazarides, and S. G. Sligar. 2004. Directed self-assembly of monodisperse phospholipid bilayer nanodiscs with controlled size. *J. Am. Chem. Soc.* **126:** 3477–3487.
16. Bayburt, T. H., Y. V. Grinkova, and S. G. Sligar. 2002. Self-assembly of discoidal phospholipid bilayer nanoparticles with membrane scaffold proteins. *Nano Lett.* **2:** 853–856.
17. Li, Y., A. Z. Kijac, S. G. Sligar, and C. M. Rienstra. 2006. Structural analysis of nanoscale self-assembled discoidal lipid bilayers by solid-state NMR spectroscopy. *Biophys. J.* **91:** 3819–3828.
18. Feng, M., A. B. Morales, T. Beugeling, A. Bantjes, K. vanderWerf, G. Gosselink, B. deGrooth, and J. Greve. 1996. Adsorption of high density lipoproteins (HDL) on solid surfaces. *J. Colloid Interface Sci.* **177:** 364–371.
19. Eisenberg, S. 1984. High-density lipoprotein metabolism. *J. Lipid Res.* **25:** 1017–1058.
20. Carlson, J. W., A. Jonas, and S. G. Sligar. 1997. Imaging and manipulation of high-density lipoproteins. *Biophys. J.* **73:** 1184–1189.
21. Jonas, A., K. E. Kezdy, and J. H. Wald. 1989. Defined apolipoprotein A-I conformations in reconstituted high-density lipoprotein disks. *J. Biol. Chem.* **264:** 4818–4824.
22. Shaw, A. W., M. A. McLean, and S. G. Sligar. 2004. Phospholipid phase transitions in homogeneous nanometer scale bilayer discs. *FEBS Lett.* **556:** 260–264.
23. Denisov, I. G., M. A. McLean, A. W. Shaw, Y. V. Grinkova, and S. G. Sligar. 2005. Thermotropic phase transition in soluble nanoscale lipid bilayers. *J. Phys. Chem. B.* **109:** 15580–15588.
24. Bacher, G., R. Korner, A. Atrih, S. J. Foster, P. Roepstorff, and G. Allmaier. 2001. Negative and positive ion matrix-assisted laser desorption/ionization time-of-flight mass spectrometry and positive ion nano-electrospray ionization quadrupole ion trap mass spectrometry of peptidoglycan fragments isolated from various Bacillus species. *J. Mass Spectrom.* **36:** 124–139.
25. Sulchek, T., G. G. Yaralioglu, C. F. Quate, and S. C. Minne. 2002. Characterization and optimization of scan speed for tapping-mode atomic force microscopy. *Rev. Sci. Instrum.* **73:** 2928–2936.
26. Caulfield, M. P., S. Li, G. Lee, P. J. Blanche, W. H. Benner, R. E. Reitz, and R. M. Krauss. 2008. Direct determination of lipoprotein particle sizes and concentrations by ion mobility analysis. *Clin. Chem.* In press.
27. Benner, W. H., R. Krauss, and P. Blanche. 2003. Ion mobility analysis of lipoproteins. U. S. Patent 7,018.
28. Morrow, J. A., D. M. Hatters, B. Lu, P. Hochtl, K. A. Oberg, B. Rupp, and K. H. Weisgraber. 2002. Apolipoprotein E4 forms a molten globule. A potential basis for its association with disease. *J. Biol. Chem.* **277:** 50380–50385.
29. Rocco, A. G., L. Mollica, E. Gianazza, L. Calabresi, G. Franceschini, C. R. Sirtori, and I. Eberini. 2006. A model structure for the heterodimer apoA-IMilano-apoA-II supports its peculiar susceptibility to proteolysis. *Biophys. J.* **91:** 3043–3049.
30. Catte, A., J. Patterson, M. Jones, W. Jerome, D. Bashtovyy, Z. Su, F. Gu, J. Chen, M. Aliste, S. Harvey, et al. 2006. Novel changes in discoidal high density lipoprotein morphology: a molecular dynamics study. *Biophys. J.* **90:** 4345–4360.
31. Wu, Z., M. A. Wagner, L. Zheng, J. S. Parks, J. M. Shy, 3rd, J. D. Smith, V. Gogonea, and S. L. Hazen. 2007. The refined structure of nascent HDL reveals a key functional domain for particle maturation and dysfunction. *Nat. Struct. Mol. Biol.* **14:** 861–868.
32. Shih, A. Y., A. Arkhipov, P. L. Freddolino, S. G. Sligar, and K. Schulten. 2007. Assembly of lipids and proteins into lipoprotein particles. *J. Phys. Chem. B.* **111:** 11095–11104.
33. Raussens, V., C. A. Fisher, E. Goormaghtigh, R. O. Ryan, and J-M. Ruysschaert. 1998. The low density lipoprotein receptor active conformation of apolipoprotein E. Helix organization in N-terminal domain-phospholipid disc particles. *J. Biol. Chem.* **273:** 25825–25830.
34. Segelke, B. W., M. Forstner, M. Knapp, S. D. Trakhanov, S. Parkin, Y. M. Newhouse, H. D. Bellamy, K. H. Weisgraber, and B. Rupp. 2000. Conformational flexibility in the apolipoprotein E amino-terminal domain structure determined from three new crystal forms: implications for lipid binding. *Protein Sci.* **9:** 886–897.
35. Davidson, W. S., and R. A. Silva. 2005. Apolipoprotein structural organization in high density lipoproteins: belts, bundles, hinges and hairpins. *Curr. Opin. Lipidol.* **16:** 295–300.
36. MacKerrell, A. D., D. Bashford, M. Bellott, R. L. Dunbrack, J. D. Evanseck, M. J. Field, S. Fischer, J. Gao, H. Guo, S. Ha, et al. 1998. All-atom empirical potential for molecular modeling and dynamics studies of proteins. *J. Phys. Chem. B.* **102:** 3586–3616.
37. Kalé, L., R. Skeel, M. Bhandarkar, R. Brunner, A. Gursoy, N. Krawetz, J. Phillips, A. Shinozaki, K. Varadarajan, and K. Schulten. 1999. NAMD2: greater scalability for parallel molecular dynamics. *J. Comput. Phys.* **151:** 283–312.
38. Law, R. J., R. H. Henchman, and J. A. McCammon. 2005. A gating mechanism proposed from a simulation of a human alpha7 nicotinic acetylcholine receptor. *Proc. Natl. Acad. Sci. USA.* **102:** 6813–6818.
39. Shih, A., I. Denisov, J. Phillips, S. Sligar, and K. Schulten. 2005. Molecular dynamics simulations of discoidal bilayers assembled from truncated human lipoproteins. *Biophys. J.* **88:** 548–556.
40. Van Der Spoel, D., E. Lindahl, B. Hess, G. Groenhof, A. E. Mark, and H. J. Berendsen. 2005. GROMACS: fast, flexible, and free. *J. Comput. Chem.* **26:** 1701–1718.
41. Humphrey, W., A. Dalke, and K. Schulten. 1996. VMD: visual molecular dynamics. *J. Mol. Graphics.* **14:** 33–38.
42. Flagan, R. C. 1998. History of electrical aerosol measurements. *Aerosol Sci. Technol.* **28:** 301–380.
43. Sparks, D. L., P. G. Frank, S. Braschi, T. A. M. Neville, and Y. L. Marcel. 1999. Effect of apolipoprotein A-I lipidation on the formation and function of pre-beta and alpha-migrating LpA-I particles. *Biochemistry.* **38:** 1727–1735.
44. Aggerbeck, L. P., J. R. Wetterau, K. H. Weisgraber, R. W. Mahley, and D. A. Agard. 1988. Crystallization and preliminary X-ray diffraction studies on the amino-terminal (receptor-binding) domain of human apolipoprotein E3 from serum very low-density lipoproteins. *J. Mol. Biol.* **202:** 179–181.
45. Aggerbeck, L. P., J. R. Wetterau, K. H. Weisgraber, C. S. C. Wu, and F. T. Lindgren. 1988. Human apolipoprotein E3 in aqueous solution. II. Properties of the amino-terminal and carboxyl-terminal domains. *J. Biol. Chem.* **263:** 6249–6258.
46. Wetterau, J. R., L. P. Aggerbeck, S. C. Rall, and K. H. Weisgraber. 1988. Human apolipoprotein E3 in aqueous solution. I. Evidence for two structural domains. *J. Biol. Chem.* **263:** 6240–6248.
47. Wilson, C., M. R. Wardell, K. H. Weisgraber, R. W. Mahley, and D. A. Agard. 1991. 3-dimensional structure of the LDL receptor-binding domain of human apolipoprotein-E. *Science.* **252:** 1817–1822.

48. Narayanaswami, V., J. N. Maiorano, P. Dhanasekaran, R. O. Ryan, M. C. Phillips, S. Lund-Katz, and W. S. Davidson. 2004. Helix orientation of the functional domains in apolipoprotein E in discoidal high density lipoprotein particles. *J. Biol. Chem.* **279:** 14273–14279.
49. Koppaka, V., L. Silvestro, J. A. Engler, C. G. Brouillette, and P. H. Axelsen. 1999. The structure of human lipoprotein A-I—evidence for the "belt" model. *J. Biol. Chem.* **274:** 14541–14544.
50. Panagotopulos, S. E., E. M. Horace, J. N. Maiorano, and W. S. Davidson. 2001. Apolipoprotein A-I adopts a belt-like orientation in reconstituted high density lipoproteins. *J. Biol. Chem.* **276:** 42965–42970.
51. Silva, R. A. G. D., G. M. Hilliard, L. Li, J. P. Segrest, and W. S. Davidson. 2005. A mass spectrometric determination of the conformation of dimeric apolipoprotein A-I in discoidal high density lipoproteins. *Biochemistry.* **44:** 8600–8607.
52. Maiorano, J. N., and W. S. Davidson. 2000. The orientation of helix 4 in apolipoprotein A-I-containing reconstituted high density lipoproteins. *J. Biol. Chem.* **275:** 17374–17380.
53. Newhouse, Y., C. Peters-Libeu, and K. H. Weisgraber. 2005. Crystallization and preliminary X-ray diffraction analysis of apolipoprotein E-containing lipoprotein particles. *Acta Crystallogr. F.* **61:** 981–984.
54. Peters-Libeu, C. A., Y. Newhouse, D. M. Hatters, and K. H. Weisgraber. 2006. Model of biologically active apolipoprotein E bound to dipalmitoylphosphatidylcholine. *J. Biol. Chem.* **281:** 1073–1079.
55. Peters-Libeu, C. A., Y. Newhouse, S. C. Hall, H. E. Witkowska, and K. H. Weisgraber. 2007. Apolipoprotein E·dipalmitoylphosphatidylcholine particles are ellipsoidal in solution. *J. Lipid Res.* **48:** 1035–1044.
56. Schneeweis, L. A., V. Koppaka, S. Lund-Katz, M. C. Phillips, and P. H. Axelsen. 2005. Structural analysis of lipoprotein E particles. *Biochemistry.* **44:** 12525–12534.
57. Li, L., J. Chen, V. K. Mishra, J. A. Kurtz, D. Cao, A. E. Klon, S. C. Harvey, G. M. Anantharamaiah, and J. P. Segrest. 2004. Double belt structure of discoidal high density lipoproteins: molecular basis for size heterogeneity. *J. Mol. Biol.* **343:** 1293–1311.
58. Jayaraman, S., D. L. Gantz, and O. Gursky. 2005. Kinetic stabilization and fusion of apolipoprotein A-2:DMPC disks: comparison with apoA-1 and apoC-1. *Biophys. J.* **88:** 2907–2918.
59. Weers, P. M. M., V. Narayanaswmi, N. Choy, R. Luty, L. Hicks, C. M. Kay, and R. O. Ryan. 2003. Lipid binding ability of human apolipoprotein E N-terminal domain isoforms: correlation with protein stability? *Biophys. Chem.* **100:** 481–492.